Coherent Anti-Stokes Raman Scattering (CARS) Microscopy: A Novel Technique for Imaging the Retina

Omid Masihzadeh,[1] David A. Ammar,[1] Malik Y. Kahook,[1] and Tim C. Lei[2]

[1]Department of Ophthalmology, University of Colorado Denver, Aurora, Colorado
[2]Department of Electrical Engineering, University of Colorado Denver, Denver, Colorado

PURPOSE. To image the cellular and noncellular structures of the retina in an intact mouse eye without the application of exogenous fluorescent labels using noninvasive, nondestructive techniques.

METHODS. Freshly enucleated mouse eyes were imaged using two nonlinear optical techniques: coherent anti-Stokes Raman scattering (CARS) and two-photon autofluorescence (TPAF). Cross sectional transverse sections and sequential flat (en face) sagittal sections were collected from a region of sclera approximately midway between the limbus and optic nerve. Imaging proceeded from the surface of the sclera to a depth of ∼60 μm.

RESULTS. The fluorescent signal from collagen fibers within the sclera was evident in the TPAF channel; the scleral collagen fibers showed no organization and appeared randomly packed. The sclera contained regions lacking TPAF and CARS fluorescence of ∼3 to 15 μm in diameter that could represent small vessels or scleral fibroblasts. Intense punctate CARS signals from the retinal pigment epithelial layer were of a size and shape of retinyl storage esters. Rod outer segments could be identified by the CARS signal from their lipid-rich plasma membranes.

CONCLUSIONS. CARS microscopy can be used to image the outer regions of the mammalian retina without the use of a fluorescent dye or exogenously expressed recombinant protein. With technical advancements, CARS/TPAF may represent a new avenue for noninvasively imaging the retina and might complement modalities currently used in clinical practice.

Keywords: multiphoton fluorescence microscopy, coherent anti-Stokes Raman scattering (CARS), retina, photoreceptors, retinal pigment epithelium (RPE)

Investigative Ophthalmology & Visual Science

Multiphoton microscopy[1-3] (MPM) differs from linear microscopy in that the emitted signal is a product of simultaneous interaction of multiple photons with the sample. Since excitation by MPM only occurs at a small focal volume, it offers intrinsic axial cross-sectioning similar to confocal microscopy.[4] However, the long wavelengths of the infrared lasers used in MPM have considerably less chance to thermally damage the sample and can be used for extended periods of time to image living tissue.[5,6] Moreover, intrinsic to the nature of MPM, the contrast mechanism is molecular specific.[2,3,7]

Two-photon autofluorescence (TPAF) is a MPM technique that has been used previously to image the retina of a live nonhuman primate.[8] However, due to low inherent autofluorescence of the tissue, long integration times were required (exceeding 12 min/image). The absence of strong near-infrared autofluorescent structures within the neural retina necessitates the addition of an exogenous fluorophore to probe the function of the intact retina. For example, fluorescent calcium-sensitive dyes have been used to detect light-induced second-messenger signaling in isolated retina.[9,10] Similarly, MPM was used to observe the in vivo cell division in the developing zebrafish retina that were transgenic for GFP-fusion proteins.[11]

Coherent anti-Stokes Raman scattering (CARS), a MPM technique based on vibrational properties of molecules,[12-15] can be tuned to detect the carbon-hydrogen bonds of lipid molecules. Since lipid membranes are common cellular structures, CARS has great utility for imaging the hydrocarbon/lipid-rich regions of biological tissues.[16-20] This property has been used extensively to visualize biological processes such as lipogenesis,[21] intracellular trafficking of lipids/proteins[21,22] as well as how cultured cells interact with three-dimensional scaffolds.[23-25] Recently, we used CARS microscopy to detect living cells and tissue structures in flat mounted ocular tissues.[26] In the present study, we have used CARS along with TPAF to image the cells and structures of the mouse sclera and retina within an intact eye without the addition of fluorescent dyes or by the use of transgenic GFP-fusion proteins.

MATERIALS AND METHODS

Sample Preparation

Mouse eyes were obtained as post-necropsy tissue from mice euthanized at the conclusion of other research projects. Adult albino mice with no known prevalence for eye diseases (BALB/C) were used. All mice were between 4 and 9 months of age. Intact eyes were first enucleated under a dissecting microscope (SMZ-800 Zoom Stereo Microscope, Nikon, Inc., Melville, NY) using a pair of curved spring scissors and excess orbital muscle tissue was subsequently removed. Eyes were placed in glass-bottom dishes (MatTek Corp., Ashland, MA) containing phosphate buffered saline (PBS; 8 g/L sodium chloride, 0.2 g/L potassium phosphate monobasic, 2.16 g/L sodium phosphate dibasic heptahydrate, pH 7.4).
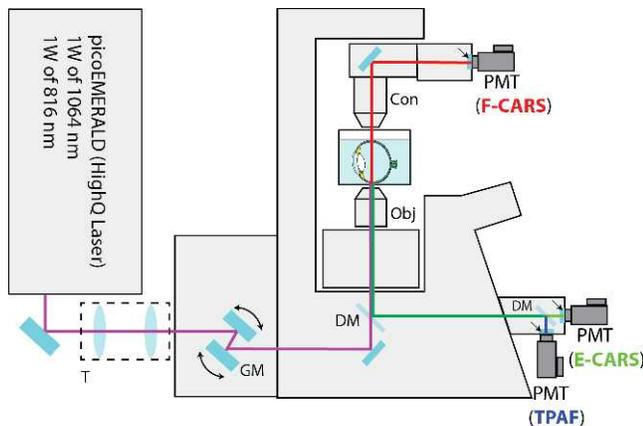
FIGURE 1. Schematic diagram of the CARS/TPAF microscope for retina imaging. The copropagating 1064 and 816 nm laser beams were telescoped down (T) and were sent to an Olympus FV-1000 confocal microscope system. The two laser beams were scanned (GM) and focused across the sample by a 60× microscope objective (Obj). The multiphoton signals (CARS and TPAF) were separated from the excitation laser beams with a dichroic mirror (DM). The E-CARS (*green*) and TPAF (*blue*) signals were detected by two PMTs in the reverse direction. The F-CARS (*red*) signal was detected in the forward direction by a third PMTs after the F-CARS signal was collected by a microscope condenser (Con). Dichroic mirrors and emission filter sets (*arrows*) were used in both epi and forward directions to separate different nonlinear signals spectrally before detection.

Imaging Mouse Tissue by CARS/TPAF Multiphoton Microscopy

The CARS/TPAF images were acquired with a custom-built MPM platform optimized for CARS and TPAF imaging shown in Figure 1.[27] The laser system (picoEMERALD, HighQ Laser, Austria) consisted of a 10 W diode-pumped Nd:Vanadate (Nd:YVO₄) picoseconds (ps) laser at a repetition rate of 80 MHz. Inside the system, 9 W of the generated 1064 nm laser beam was redirected to a frequency doubling crystal to produce 5 W of 532 nm light which was subsequently sent into an optical parametric oscillator to convert the 532 nm laser beam into a 1 W, ~6 ps, 816 nm laser beam. The remaining 1 W of the 1064 nm beam (Stokes) from the Nd:Vanadate laser was then optically recombined with the 816 nm optical beam (pump and probe) and sent into an Olympus FV-1000 confocal microscope platform (Olympus, Center Valley, PA) for CARS and TPAF imaging. The powers of the two laser beams delivered to the microscope was adjusted inside the laser system. The optical power at the objective (UPSLAPO 60× IR W, Olympus) was 16.5 mW for the 816 nm laser beam and 15.0 mW for the 1064 nm laser beam; both settings are below the tissue damage threshold.[28]

Imaging Mouse Tissue

In all cases, imaging was performed on whole mouse eyes and not dissected tissue (i.e., retina or sclera). Intact mouse eyes on the glass bottom dishes were placed on a microscope stage in a humidity/temperature controlled chamber. Eyes were oriented along a horizontal line connecting the optic nerve with the corneal apex. This placed the microscope objective facing an equatorial region of sclera approximately midway between the optic nerve and limbus. Imaging was performed on an inverted microscope (FV-1000, Olympus) equipped with four external photomultiplier detectors (PMTs): two detectors in the epi-direction (reverse orientation) collecting signal through the objective lens and the other two detectors in the forward

direction collecting signal through the microscope condenser. A dichroic mirror (595dcxr, Chroma Technology Corp., Bellows Falls, VT) was used in the epi-direction to separate the TPAF signal from the epi-CARS signal. The TPAF signal (between 420–520 nm) was collected by the first epi-PMT through an emission filter (hp470/100m-2p, Chroma Technology Corp.). The epi-CARS signal (between 640–680 nm) was collected by the second epi-PMT using an emission filter (hq660/40m-2p; Chroma Technology Corp.). The forward CARS signal (between 640–680 nM) was collected with a condenser and filtered by another emission filter (hq660/40m-2p) located in front of the forward PMT. The pixel dwell time was 10 μs and the image pixel resolution was 800 × 800 when acquiring xy stacks and 1018 × 3000 for line (xz) scans. A Kalman average filter ($n = 3$ for xy stacks and $n = 10$ for line scans) was applied during image acquisitions to improve the signal-to-noise ratio of the acquired images.

Image Analysis and Processing

The Olympus FV-1000 software package was used to collect all images. Acquired images were post-processed for background noise (nonresonant background) reduction and prepared as its current format by ImageJ (http://rsbweb.nih.gov/ij/) software. Where applicable, tiling of the line-scans was accomplished by Adobe Illustrator (Adobe, San Jose, CA).

RESULTS

Imaging by Transverse Sectioning

The retinas of intact mouse eyes were imaged through the overlying sclera by TPAF and CARS microscopy. Line scans were performed perpendicular to the surface of the sclera, centered at a region ~1 mm from the limbus. Scanning began at the surface (defined by the sharp increase in signal seen in 2PAF and CARS detectors) and extended >60 μm interior to the surface of the sclera along an axis that would correspond to a sagittal/transverse histological section. A representative section is shown in Figure 2, with TPAF structures shown in blue and the CARS signals from the forward detector (F-CARS) and epi-detector (E-CARS) shown in red and green, respectively. A significant F-CARS signal is noticeable at the surface of the eye (~2–4 μm deep) and may represent the lipid membranes of bulbar conjunctiva (Fig. 2D, 'Co'). Bands of material 2 to 3 μm thick with both F-CARS and E-CARS signal (Figs. 2B, 2C) appear throughout the surface region of the eye 18 to 20 μm thick that should correspond to the sclera. These may represent lipid deposits within the sclera seen with aging,[29] or may represent nonresonant signal from the dense scleral tissue.[12] The signal from E-CARS is significantly weaker than the signal from F-CARS (Fig. 2C vs. 2B). E-CARS signal from the sclera is detectable but individual fibrous strands are not discernible. Also visible in the F- but not E-CARS channel are rod-shaped structures approximately 42 to 56 μm interior to the surface of the sclera. The size (diameter approximately 1–2 μm), shape, and orientation of these structures, along with the fact that they have a lipid-rich CARS signal, argue that these are the membrane-dense photoreceptor outer segments (Fig. 2D, 'P'). Intense punctate signal are seen in both F- and E-CARS from structures ~36 to 40 μm interior to the surface of the tissue. By correlating the position of this band to the structures that appear to be rod outer segments, these punctate lipid structures should be located within the retinal pigment epithelium (RPE).

The most prominent structures seen with TPAF in these line scans (Fig. 2A) are repeated 2 to 3 μm-thick bands of material
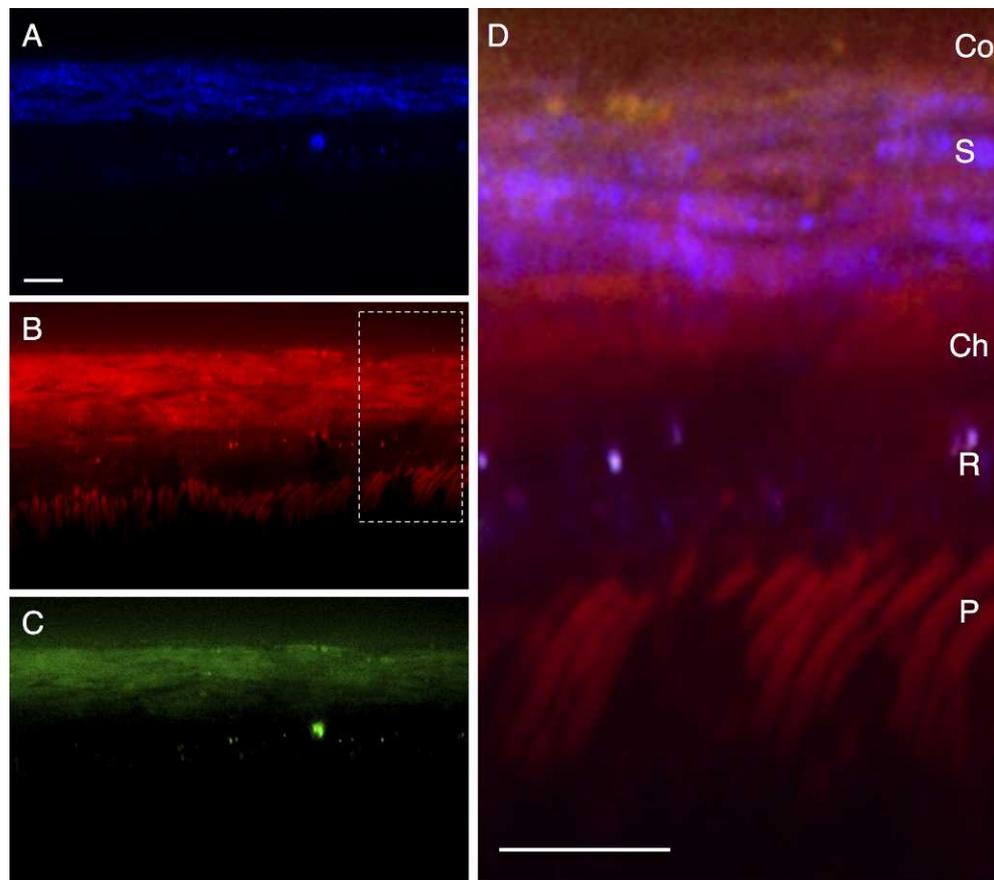
FIGURE 2. Line scan of a posterior region of a mouse eye, representing a transverse/sagittal section. The conjunctiva (Co) is located at the top of the images, with retinal photoreceptors (P) located at the bottom. (**A**) shows two-photon autofluorescence (TPAF) in *blue*. The coherent anti-Stokes Raman scattering (CARS) signal from the forward detector (F-CARS, *red*) is shown in (**B**) and from the epi-detector (E-CARS, *green*) in (**C**). Both CARS and TPAF signals are overlapped in (**D**). S, sclera; Ch, choroid; R, RPE; P, photoreceptors. *Scale bar*: 10 μm.

near the surface of the eye. These most likely represent the structural collagen fibers within the sclera. A second, weaker TPAF band is located interior to the sclera (separated by a ~6 μm region lacking TPAF) which is presumably the RPE. Intense, punctate TPAF spots are located in this region, overlapping the position of both F- and E-CARS, suggested that these lipid structures within the RPE have fluorescent properties.

Imaging by Sagittal Sectioning

We also performed cross-section scans at various depths interior to the surface of the sclera. In scans located within 2 μm of the surface region of the mouse eye, occasional bright round structures appear in the F- and E-CARS channels (Fig. 3A). These structures are ~15 μm in size, and are likely flattened bulbar conjunctival cells or perhaps a surface fibroblast. Scans within the sclera region of the mouse eye (~15 μm interior to the tissue surface) show the collagen fibers (Fig. 3B, blue TPAF channel) as repeated strands of material interwoven into one another. Occasional dark regions (~3–15 μm across) appear within the sclera (Fig. 3B). Since these regions lack both CARS and TPAF signal, these are most likely fluid-filled spaces.

Figure 4A shows a cross-section ~25 μm interior to the surface of the eye, in the approximate region of the choroid. Tissue in this region lacks strong TPAF signal (blue), but round lipid-rich structures are apparent in the F-CARS channel (red). Some of these objects have the disk-shaped structure of red

blood cells, and many of these cells are tightly packed in a linear arrangement suggesting that this region contains the capillary blood vessels adjacent to the RPE. A cross-section performed 11 μm adjacent to Figure 4A at the level of the RPE is shown in Figure 4B. Dark regions lacking fluorescent signal occur with the size and spacing of RPE nuclei. Small white structures, a chromatic combination of the strong signals from both CARS channels (red and green) as well as the TPAF (blue) channel, are also visible and may represent intracellular retinyl ester stores. The cross-section in Figure 5A is located 2 μm from Figure 4B, traveling through the apical region of the RPE. The tight-junctions of the RPE, with their characteristic hexagonal shape, are visible in the E-CARS channel (green, Fig. 5A). The cross-section shown in Figure 5B is located 4 μm apically from section in Figure 5B. Figure 5B shows the transition of the RPE tight junctions on the left (E-CARS, green) to the lipid-rich RPE microvilli in the center (F-CARS, red) to the distal ends of the photoreceptor outer segments on the right (F-CARS, red).

At the deepest region imaged we see the cross-sections of the outer region of the photoreceptor layer. Figures 6A and 6B (~49 and 55 μm interior to the surface of the eye) travel through the distal end and middle region of the photoreceptor outer segments, respectively. The membrane-dense rod outer segments (~2 μm in diameter) have a strong F-, but not E-CARS signal. Occasional dark spaces within the outer segments (*) likely represent the location of cone photoreceptors. These dark spaces (~2–4 μm across) occur at a frequency of
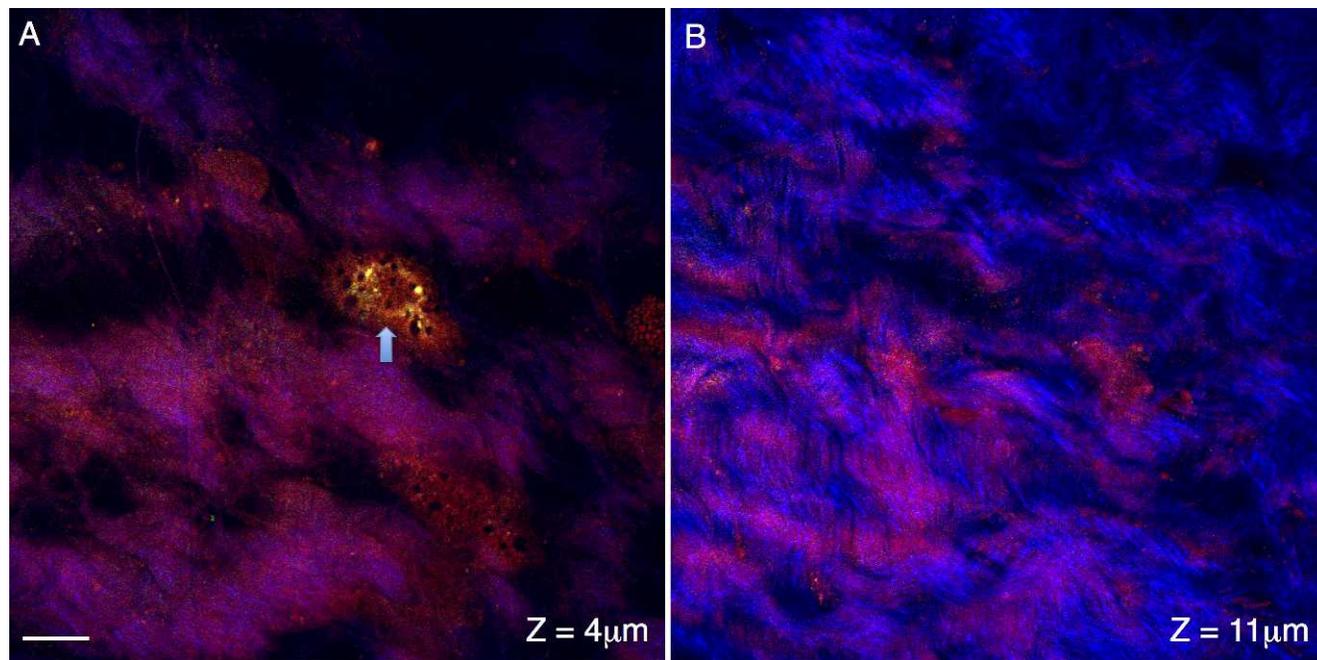
FIGURE 3. Cross-sections of conjunctival and sclera regions of the posterior mouse eye. Signal from the forward coherent anti-Stokes Raman scattering detector (F-CARS, *red*), epi-detector (E-CARS, *green*) and two-photon autofluorescence (TPAF, *blue*) are shown. The cross-section in (**A**) shows the surface region of the mouse eye ~4 μm from the surface of the tissue. A surface cell is apparent in the CARS channels (*arrow*) and is likely a bulbar conjunctival cell but may be a scleral fibroblast. The cross-section in (**B**) travels through the mouse sclera (~11 μm from the tissue surface). The collagen fibers appear in the TPAF channel as repeated strands of material interwoven into one another. *Scale bar*: 10 μm.

approximately 1 per 30 to 40 rod photoreceptors, which is in the range of 1 cone per 35 rod photoreceptor reported by Jeon et al.[30] The entire region of photoreceptors visible by F-CARS is approximately 14 to 19 μm thick.

An animation containing a total of 51 cross-sections (spaced 1 μm apart) is shown in Supplementary Movie S1. The animation begins at the surface of the mouse sclera, where the signal from the F- and E-CARS (combining to yellow) is
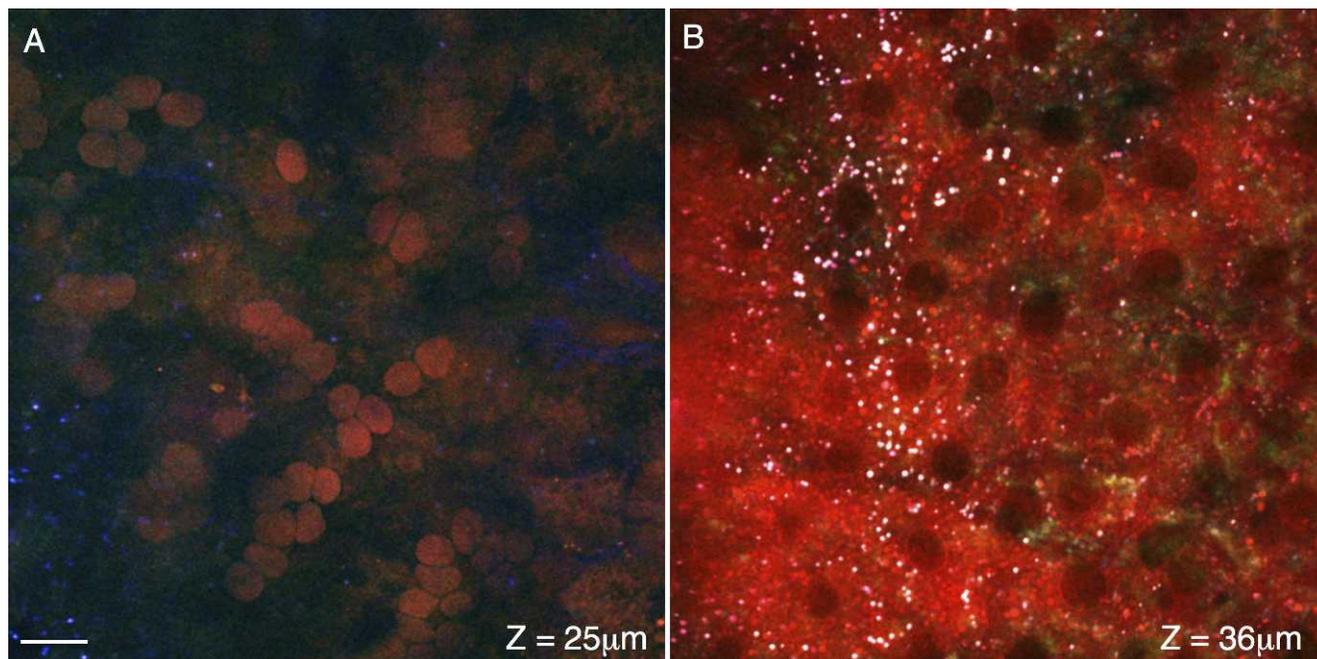

FIGURE 4. Cross-sections of the choroid and retinal pigment epithelium. Signal from the forward coherent anti-Stokes Raman scattering detector (F-CARS, *red*), epi-detector (E-CARS, *green*), and two-photon autofluorescence (TPAF, *blue*) are shown. A cross-section of choroid is shown in (**A**), located approximately 25 μm from the tissue surface. The spherical objects with F-CARS signal are likely red blood cells within the choriocapillaris. The cross-section in (**B**) travels through a RPE, approximately 36 μm from the surface of the tissue. Dark regions lacking CARS/TPEF signal are of a size and spacing to be nuclei. Punctate objects (~1 μm) with strong CARS/TPEF signal (*white* due to the chromatic combination of the *red/green/blue* channels) may represent retinyl ester storage structures. *Scale bar*: 10 μm.
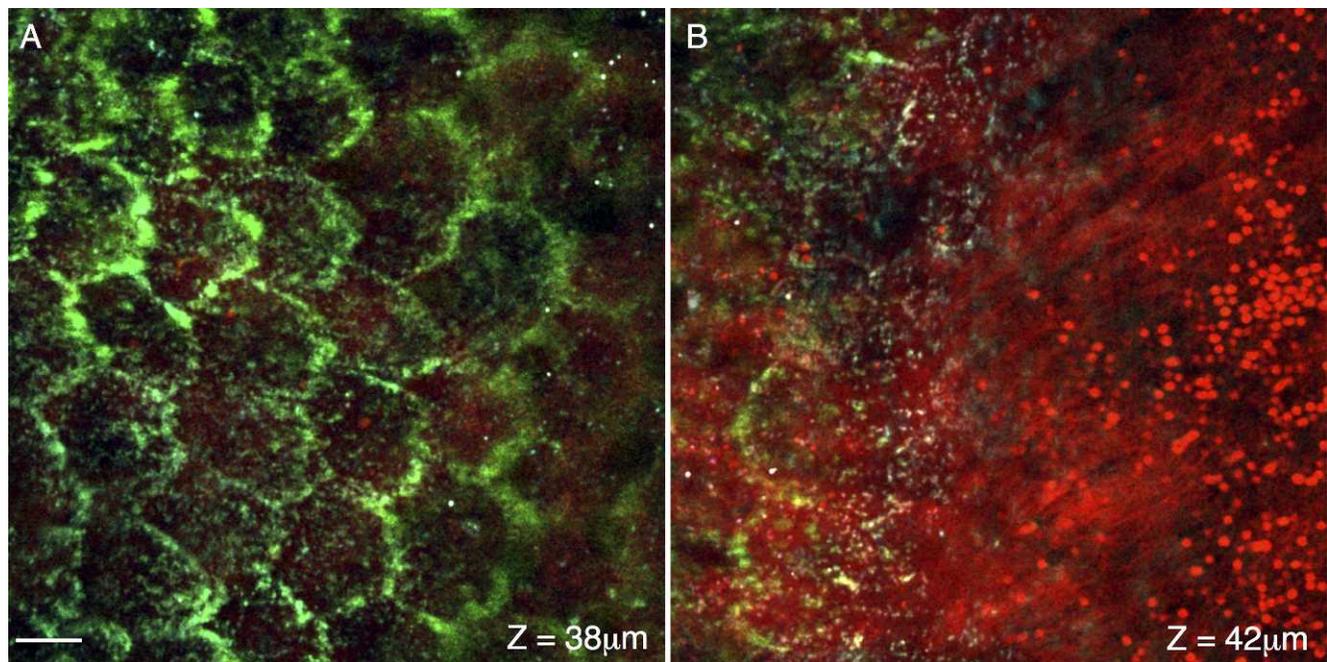
FIGURE 5. Cross-sections at the boundary of the retinal pigment epithelium and photoreceptors. Signal from the forward coherent anti-Stokes Raman scattering detector (F-CARS, *red*), epi-detector (E-CARS, *green*), and TPAF (*blue*) are shown. (**A, B**) are located approximately 38 and 42 μm from the surface of the eye. The tight-junctions of the RPE, with their characteristic hexagonal shape, are visible in the E-CARS channel (*green*, [**A**]). (**B**) shows the transition of the RPE tight junctions (*left, green*) to the lipid-rich RPE microvilli (*center, red*) to the distal ends of the photoreceptor outer segments (*red, right*). *Scale bar*: 10 μm.

visible nestled between the TPAF signal from the collagen fibers (blue). As the animation progresses into the sclera, the TPAF collagen signal dominates, and the bundles of collagen fibers become more apparent. In our imaging, the choroid appears next as a region lacking TPAF fluorescence, but with an intense layer of F-CARS signal. This may represent the suprachoroid lamina region containing pigment and connective tissue. Deeper within the choroid are spherical F-CARS structures that may be red blood cells (seen in Fig. 4A). Beneath the choroid layer is the RPE layer, containing are small
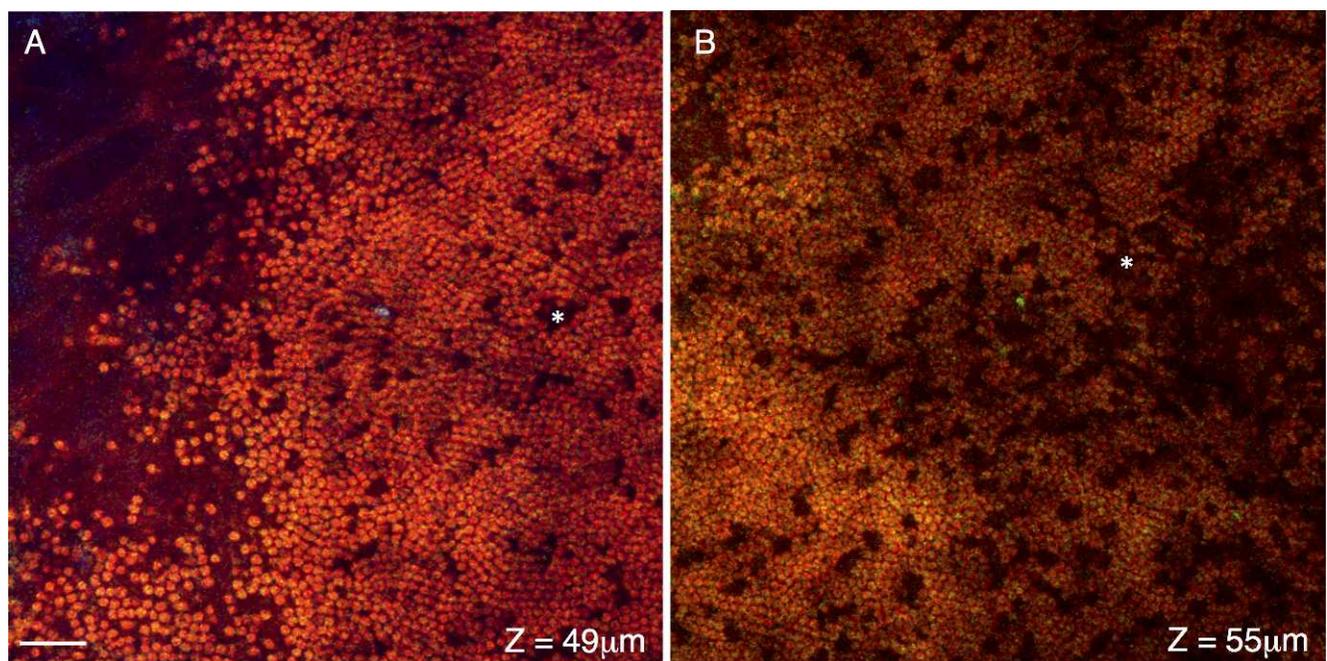

FIGURE 6. Cross-sections of the distal ends of the photoreceptor layer. Signal from the F-CARS (*red*), E-CARS (*green*), and TPAF (*blue*) are shown. Cross-sections shown in (**A, B**) are located approximately 49 and 55 μm interior to the surface of the eye, travel through the distal and middle regions of the photoreceptor outer segments, respectively. These lipid rich disks generate a strong F- but not E-CARS signal. Occasional dark spaces within the outer segments (*) likely represent the location of cone photoreceptors. *Scale bar*: 10 μm.
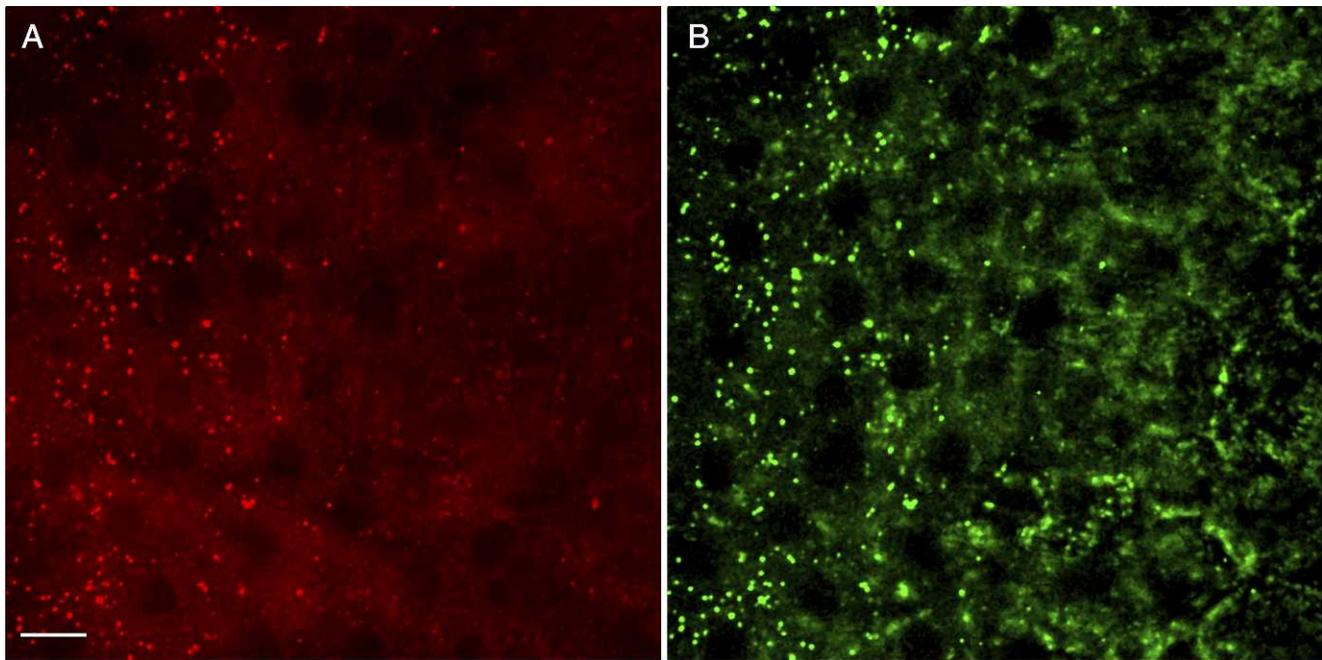
Investigative Ophthalmology & Visual Science

FIGURE 7. Differences in F- and E- CARS signals are due to size, shape and composition of target structures. (**A, B**) are taken from a cross-section through the RPE, approximately 37 μm interior to the surface of the eye. Signal from the F-CARS (*red*) is shown in (**A**), and signal from the E-CARS (*green*) is shown in (**B**). Smaller (>1 μm) lipid structures, such as retinyl ester storage structures, generate a strong F- and E-CARS signal. *Scale bar*: 10 μm.

(∼1 μm) objects that stain intensely with TPAF and both F- and E-CARS. These are presumably intracellular retinyl storage structures seen in Figure 4B. The next structures that appear are CARS-rich hexagonal structures that may represent the tight junctions of the RPE (seen in Fig. 5A). Finally, the photoreceptor outer segments appear as lipid-rich hexagonal/round structures as shown in Figures 6A and 6B. Supplementary Movie S2 is the 3D rendering of same data used in Supplementary Movie S1.

DISCUSSION

Multiphoton microscopy (MPM) has the ability to image the function and structure of cells and tissues without exogenous dyes. This label-free imaging relies on simultaneous interactions of multiple photons with target material. These interactions involve a resonant or nonresonant excitation of one of the basic energy states: electronic or vibrational energies. Unlike traditional microscopy where a single photon interacts with material (through scattering or absorption), MPM uses pulsed infrared laser light to generate signal from a sample through simultaneous absorption or scattering of two or more photons. In TPAF, two photons from a single laser are simultaneously absorbed and excite the molecule to its higher *electronic state*. After nonradiative relaxation, the molecule returns to its electronic ground state through the release of a fluorescent photon. In CARS, two laser beams with different optical wavelengths simultaneously and resonantly excite the *vibrational states* of carbon-hydrogen bonds in an ensemble of lipid molecules in a coherent fashion. This ultimately results in the release of optical photons in a direction that is dependent on the size and shape of the lipid object.

The two lasers in the MPM system can generate resonant (CARS) and nonresonant (background) signals. This nonresonant signal is clearly visible in the sclera images in Figures 2B and 2C, where abundant amount of CARS signals are recorded where no significant lipids should be present. A distinction between the resonant from nonresonant signal can be differentiated, however, by detuning the lasers from the vibrational band, as the resonant signal is going to vanish and the nonresonant background signal will dominate. There are several methods suggested for background discrimination in CARS microscopy and it has been documented in detail.[31] On the other hand, this nonresonant signal can be advantageous for visualizing structures where the tissue does not autofluoresce.

In our previous work we have used MPM techniques (TPAF and second harmonic generation) to perform deep-tissue imaging of the anterior chamber of the intact human and mouse eye.[27,32-34] In this study, we have focused on imaging deeply into the posterior chamber of the mouse eye by imaging through the sclera into the photoreceptor outer segments. Our TPAF images of the mouse sclera are qualitatively similar to the images of pig sclera performed by Wang et al.,[35] showing distinct bands of collagenous fibers (∼2 μm wide) undulating and interweaving into one another. Additionally, we see multiple intracellular autofluorescent structures within the RPE cell layer that also are visible in the CARS channels, indicating that they have a lipid signature. These structures are similar to those seen previously by others,[35,36] and most likely represent retinal ester storage particles (REST) imaged by TPAF in intact mouse eyes.[37] Imanishi et al. used MPM to determine that these intracellular structures were oblong in shape (∼1 μm in diameter), with a characteristic fluorescence of retinyl esters (excitation 330 nm; emission 490 nm).[38] Due to the young age of the animals, we do not believe these structures are lipofuscin particles seen with TPAF in aged human RPE.[39]

In this study we demonstrate the utility of CARS/TPAF microscopy in identifying structures of the outer retina in intact tissue that are not visible by TPAF and second harmonic generation microscopy performed previously. In general, while the signals from F-CARS and E-CARS are qualitatively the same, the signal intensity is greatest in the F-CARS. This is due to the

fact that unlike TPAF, the directionality of CARS signal is dependent on the size and shape of the target.[12] For spherical structures that are much smaller than the wavelength of the Stokes/pump lasers, F- and E-CARS signals are equal. The small lipid particles within the RPE cell layer demonstrate this phenomenon (Fig. 7). The small (<1 μm) retinyl esters storage structures appear equally bright in both the F-CARS (Fig. 7A) and E-CARS (Fig. 7B). While the overall E-CARS signal within the sclera is faint, only the smaller structures within the RPE generate a strong E-CARS signal. In contrast, in the nearby sections the larger (~2 μm) lipid-rich photoreceptor outer segments show strong F-CARS but not E-CARS signal (Figs. 6A, 6B, lack of green signal). Additionally, while the signal from E-CARS may be weaker, the structures visible in the E-CARS channel can be more distinct than F-CARS due to a reduced nonresonant background signal from water.[40]

We recognize that we have not verified the structures and cell types using optical coherence tomography or standard histological/immunofluorescent techniques. In the latter case, we have found that histological processing alters the physical properties of the tissues such that subsequent CARS images appear qualitatively different to images from fresh tissue. Therefore, dual imaging by CARS and immunofluorescence is not currently available to us, although we are working to overcome this technical issue. However based on size and location of these structures, we believe that our cellular identifications are correct. For example, electron microscopy images of mouse retina show that the rods outer segments extend 10 to 15 μm beyond the tips of the cones.[41] This would explain the cross sections in Figure 6, which show a strong mosaic of rod outer segments interspersed with empty spaces. These spaces are of a size and frequency to correspond to the locations of the shorter cones, and are a compelling argument that we are indeed imaging the rod outer segments of the retina.

In conclusion, we propose that this technique can be used to image outer retinal tissue from the mouse eye, including established disease models, without the need for introducing a fluorescently tagged protein. Furthermore, CARS has potential to add useful information particularly when combined with other nonlinear microscopic techniques. For example, nonlinear microscopy has been used to analyze the collagen fibers within the optic nerve head in response to increased ocular pressure in an enucleated eye.[42] Brown et al. were able to determine that the open spaces within the collagen matrix of the lamina cribrosa do not respond uniformly; instead, the largest and most peripheral pores compress the most. Previous studies have also used CARS and TPAF to study the cycle of 11-cis retinol diffusion and light-induced photoisomerization in isolated rod outer segments.[43,44] The work presented here may subsequently lead to in vivo imaging experiments which monitor the recycling of retinol within the living mouse eye, giving further insight into retinal function and dysfunction.

Acknowledgments

Disclosure: **O. Masihzadeh**, P; **D.A. Ammar**, P; **M.Y. Kahook**, P; **T.C. Lei**, P

References

1. Denk W, Strickler JH, Webb WW. Two-photon laser scanning fluorescence microscopy. *Science*. 1990;248:73–76.

2. Helmchen F, Denk W. Deep tissue two-photon microscopy. *Nat Methods*. 2005;2:932–940.

3. Pezacki JP, Blake JA, Danielson DC, Kennedy DC, Lyn RK, Singaravelu R. Chemical contrast for imaging living systems: molecular vibrations drive CARS microscopy. *Nat Chem Biol*. 2011;7:137–145.

4. Cox G, Sheppard CJ. Practical limits of resolution in confocal and non-linear microscopy. *Microsc Res Tech*. 2004;63:18–22.

5. So PT, Dong CY, Masters BR, Berland KM. Two-photon excitation fluorescence microscopy. *Annu Rev Biomed Eng*. 2000;2:399–429.

6. So P, Kim H, Kochevar I. Two-photon deep tissue ex vivo imaging of mouse dermal and subcutaneous structures. *Opt Express*. 1998;3:339–350.

7. Gibson EA, Masihzadeh O, Lei TC, Ammar DA, Kahook MY. Multiphoton microscopy for ophthalmic imaging. *J Ophthalmol*. 2011;2011:870879.

8. Hunter JJ, Masella B, Dubra A, et al. Images of photoreceptors in living primate eyes using adaptive optics two-photon ophthalmoscopy. *Biomed Opt Express*. 2010;2:139–148.

9. Denk W, Detwiler PB. Optical recording of light-evoked calcium signals in the functionally intact retina. *Proc Natl Acad Sci U S A*. 1999;96:7035–7040.

10. Gray-Keller M, Denk W, Shraiman B, Detwiler PB. Longitudinal spread of second messenger signals in isolated rod outer segments of lizards. *J Physiol*. 1999;519:679–692.

11. Das T, Payer B, Cayouette M, Harris WA. In vivo time-lapse imaging of cell divisions during neurogenesis in the developing zebrafish retina. *Neuron*. 2003;37:597–609.

12. Cheng JX, Xie XS. Coherent anti-Stokes Raman scattering microscopy: instrumentation, theory, and applications. *J Phys Chem B*. 2004;108:827–840.

13. Potma EO, de Boeij WP, Wiersma DA. Nonlinear coherent four-wave mixing in optical microscopy. *J Opt Soc Am B*. 2000;17: 1678–1684.

14. Zumbusch A, Holtom GR, Xie XS. Three-dimensional vibrational imaging by coherent anti-Stokes Raman scattering. *Phys Rev Lett*. 1999;82:4142–4145.

15. Xie XS, Yu J, Yang WY. Living cells as test tubes. *Science*. 2006; 312:228–230.

16. Huff TB, Cheng JX. In vivo coherent anti-Stokes Raman scattering imaging of sciatic nerve tissue. *J Microsc*. 2007;225: 175–182.

17. Wang HW, Le TT, Cheng JX. Label-free imaging of arterial cells and extracellular matrix using a multimodal CARS microscope. *Opt Commun*. 2008;281:1813–1822.

18. Evans CL, Potma EO, Puoris'haag M, Cote D, Lin CP, Xie XS. Chemical imaging of tissue in vivo with video-rate coherent anti-Stokes Raman scattering microscopy. *Proc Natl Acad Sci U S A*. 2005;102:16807–16812.

19. Fu Y, Huff TB, Wang HW, Wang HF, Cheng JX. Ex vivo and in vivo imaging of myelin fibers in mouse brain by coherent anti-Stokes Raman scattering microscopy. *Opt Express*. 2008;16: 19396–19409.

20. Lin CY, Suhalim JL, Nien CL, et al. Picosecond spectral coherent anti-Stokes Raman scattering imaging with principal component analysis of meibomian glands. *J Biomed Opt*. 2011;16.

21. Rakic B, Sagan SM, Noestheden M, et al. Peroxisome proliferator-activated receptor alpha antagonism inhibits hepatitis C virus replication. *Chem Biol*. 2006;13:23–30.

22. Tong L, Lu Y, Lee RJ, Cheng JX. Imaging receptor-mediated endocytosis with a polymeric nanoparticle-based coherent anti-Stokes Raman scattering probe. *J Phys Chem B*. 2007;111: 9980–9985.

23. Kaufman LJ, Brangwynne CP, Kasza KE, et al. Glioma expansion in collagen I matrices: analyzing collagen concentration-dependent growth and motility patterns. *Biophys J*. 2005;89:635–650.

24. Conovaloff A, Wang HW, Cheng JX, Panitch A. Imaging growth of neurites in conditioned hydrogel by coherent anti-Stokes Raman scattering microscopy. *Organogenesis*. 2009;5:231–237.

25. Brackmann C, Esguerra M, Olausson D, et al. Coherent anti-Stokes Raman scattering microscopy of human smooth muscle cells in bioengineered tissue scaffolds. *J Biomed Opt*. 2011;16: 021115.

26. Lei TC, Ammar DA, Masihzadeh O, Gibson EA, Kahook MY. Label-free imaging of trabecular meshwork cells using coherent anti-Stokes Raman scattering (CARS) microscopy. *Mol Vis*. 2011;17:2628–2633.

27. Ammar DA, Lei TC, Masihzadeh O, Gibson EA, Kahook MY. Trans-scleral imaging of the human trabecular meshwork by two-photon microscopy. *Mol Vis*. 2011;17:583–590.

28. Potma E. Tissue imaging with coherent anti-Stokes Raman scattering microscopy. In: Srinivasan G, ed. *Vibrational Spectroscopy Imaging for Biomedical Application*. Columbus, OH: McGraw-Hill Professional; 2010: 319–348.

29. Haimovici R, Gantz DL, Rumelt S, Freddo TF, Small DM. The lipid composition of drusen, Bruch's membrane, and sclera by hot stage polarizing light microscopy. *Invest Ophthalmol Vis Sci*. 2001;42:1592–1599.

30. Jeon CJ, Strettoi E, Masland RH. The major cell populations of the mouse retina. *J Neurosci*. 1998;18:8936–8946.

31. Min W, Freudiger CW, Lu S, Xie XS. Coherent nonlinear optical imaging: beyond fluorescence microscopy. *Annu Rev Phys Chem*. 2011;62:507–530.

32. Johnson AW, Ammar DA, Kahook MY. Two-photon imaging of the mouse eye. *Invest Ophthalmol Vis Sci*. 2011;52:4098–4105.

33. Masihzadeh O, Ammar DA, Kahook MY, Gibson EA, Lei TC. Direct trabecular meshwork imaging in porcine eyes through multiphoton gonioscopy. *J Biomed Opt*. 2013;18:036009.

34. Masihzadeh O, Lei TC, Ammar DA, Kahook MY, Gibson EA. A multiphoton microscope platform for imaging the mouse eye. *Mol Vis*. 2012;18:1840–1848.

35. Wang BG, Eitner A, Lindenau J, Halbhuber KJ. High-resolution two-photon excitation microscopy of ocular tissues in porcine eye. *Lasers Surg Med*. 2008;40:247–256.

36. La Schiazza O, Bille JF. High-speed two-photon excited autofluorescence imaging of ex vivo human retinal pigment epithelial cells toward age-related macular degeneration diagnostic. *J Biomed Opt*. 2008;13:064008.

37. Imanishi Y, Sun W, Maeda T, Maeda A, Palczewski K. Retinyl ester homeostasis in the adipose differentiation-related protein-deficient retina. *J Biol Chem*. 2008;283:25091–25102.

38. Imanishi Y, Palczewski K. Visualization of retinoid storage and trafficking by two-photon microscopy. *Methods Mol Biol*. 2010;652:247–261.

39. Han M, Bindewald-Wittich A, Holz FG, et al. Two-photon excited autofluorescence imaging of human retinal pigment epithelial cells. *J Biomed Opt*. 2006;11:010501.

40. Volkmer A, Cheng JX, Xie XS. Vibrational imaging with high sensitivity via epidetected coherent anti-Stokes Raman scattering microscopy. *Phys Rev Lett*. 2001;87:023901–024904.

41. Carter-Dawson LD, LaVail MM. Rods and cones in the mouse retina. I. Structural analysis using light and electron microscopy. *J Comp Neurol*. 1979;188:245–262.

42. Brown DJ, Morishige N, Neekhra A, Minckler DS, Jester JV. Application of second harmonic imaging microscopy to assess structural changes in optic nerve head structure ex vivo. *J Biomed Opt*. 2007;12:024029.

43. Ujj L, Jager F, Atkinson GH. Vibrational spectrum of the lumi intermediate in the room temperature rhodopsin photoreaction. *Biophys J*. 1998;74:1492–1501.

44. Wu Q, Chen C, Koutalos Y. All-trans retinol in rod photoreceptor outer segments moves unrestrictedly by passive diffusion. *Biophys J*. 2006;91:4678–4689.